Geophysical Research Letters

RESEARCH LETTER
10.1029/2023GL106716

Spatial and Temporal Patterns of Southern Ocean Ventilation

Andrew F. Styles[1], Graeme A. MacGilchrist[2], Michael J. Bell[3], and David P. Marshall[1]

[1]Department of Physics, University of Oxford, Oxford, UK, [2]Program in Atmospheric and Oceanic Science, Princeton University, Princeton, NJ, USA, [3]Met Office, Exeter, UK

Key Points:

- Extensive backwards-in-time trajectories are used to explore the 30 year history of ventilation in a simulated Southern Ocean
- Local hotspots only account for a fraction of Southern Ocean ventilation (60%), the remaining ventilation occurs in a circumpolar pattern
- Almost all Southern Ocean ventilation occurs between August and November while the mixed layer is shoaling

Correspondence to:
A. F. Styles,
afstylesocean@gmail.com

Citation:
Styles, A. F., MacGilchrist, G. A., Bell, M. J., & Marshall, D. P. (2024). Spatial and temporal patterns of Southern Ocean Ventilation. *Geophysical Research Letters*, *51*, e2023GL106716. https://doi.org/10.1029/2023GL106716

Received 11 OCT 2023
Accepted 24 JAN 2024

Abstract Ocean ventilation translates atmospheric forcing into the ocean interior. The Southern Ocean is an important ventilation site for heat and carbon and is likely to influence the outcome of anthropogenic climate change. We conduct an extensive backwards-in-time trajectory experiment to identify spatial and temporal patterns of ventilation. Temporally, almost all ventilation occurs between August and November. Spatially, "hotspots" of ventilation account for 60% of open-ocean ventilation on a 30 years timescale; the remaining 40% ventilates in a circumpolar pattern. The densest waters ventilate on the Antarctic shelf, primarily near the Antarctic Peninsula (40%) and the west Ross sea (20%); the remaining 40% is distributed across East Antarctica. Shelf-ventilated waters experience significant densification outside of the mixed layer.

Plain Language Summary Only a small fraction of the ocean is interacting with the atmosphere at any given time. This water is definitively found in the upper mixing layer of the ocean. When this water leaves the mixing layer and enters the ocean interior, it has "ventilated" (this term arising from the abundance of oxygen in newly ventilated water). The Southern Ocean is an important region for ventilation, and the uptake of heat and carbon dioxide there is likely to influence the limits and timescales of climate change. By calculating the 30 year history of over 480 million fluid parcels, we find that 60% of open-ocean ventilation occurs in certain "hotspots" and almost exclusively between August and November.

1. Introduction

Ocean ventilation describes how mixed layer properties such as temperature, salinity, and dissolved gas concentrations are translated into the interior ocean. The Southern Ocean is an important area for the ventilation of intermediate and abyssal waters (Gebbie & Huybers, 2010) and is also where much of the deep water formed in the North Atlantic returns to the surface to interact with the atmosphere (Liu & Huang, 2012; Talley, 2013). The ventilation of heat and carbon in the Southern Ocean is expected to influence the limits and timescale of anthropogenic climate change (Bopp et al., 2002; Sallée et al., 2012) and it is therefore important to work out where and when the Southern Ocean ventilates.

Subduction is the transfer of water from the mixed layer into the interior ocean and is often assumed to be a rate-limiting step for Southern Ocean ventilation. Localized subduction "hotspots" can be identified in Argo data (Sallée et al., 2010, 2012) and reanalysis (Buongiorno Nardelli et al., 2018). These sites have deep mixed layers in late winter and undoubtedly influence the ventilation of the Southern Ocean. However, the ventilating effect of subducted water also depends on the timescale of re-entrainment by the mixed layer which is uncertain near these sites (Jones et al., 2016) and can be influenced by ocean currents (Jones et al., 2019). Re-entrained water has no long term influence on the heat (e.g., Frölicher et al., 2015), carbon (Sallée et al., 2010), or nutrient (Sarmiento et al., 2004) budgets of the global interior ocean. Here, we study the spatial and temporal patterns of ventilation using a method that considers the dynamics of subduction and re-entrainment.

Extensive backwards-in-time trajectory experiments reveal the history of the interior ocean including a record of the position and timing of ventilation. For example, MacGilchrist et al. (2020) find that 60% of ventilation in the Labrador Sea occurs within the boundary current and only 20% arises from deep ocean convection. Ventilation sites do not require deep mixed layers when the dynamics of subduction, re-entrainment, and ocean currents are considered. Using similar methodology, MacGilchrist et al. (2021) find that the North Atlantic almost entirely ventilates in late winter, in agreement with the earlier passive tracer experiment by Williams et al. (1995) and the theory of "Stommel's Demon" (Stommel, 1979). The demon has enabled simpler models of the ocean

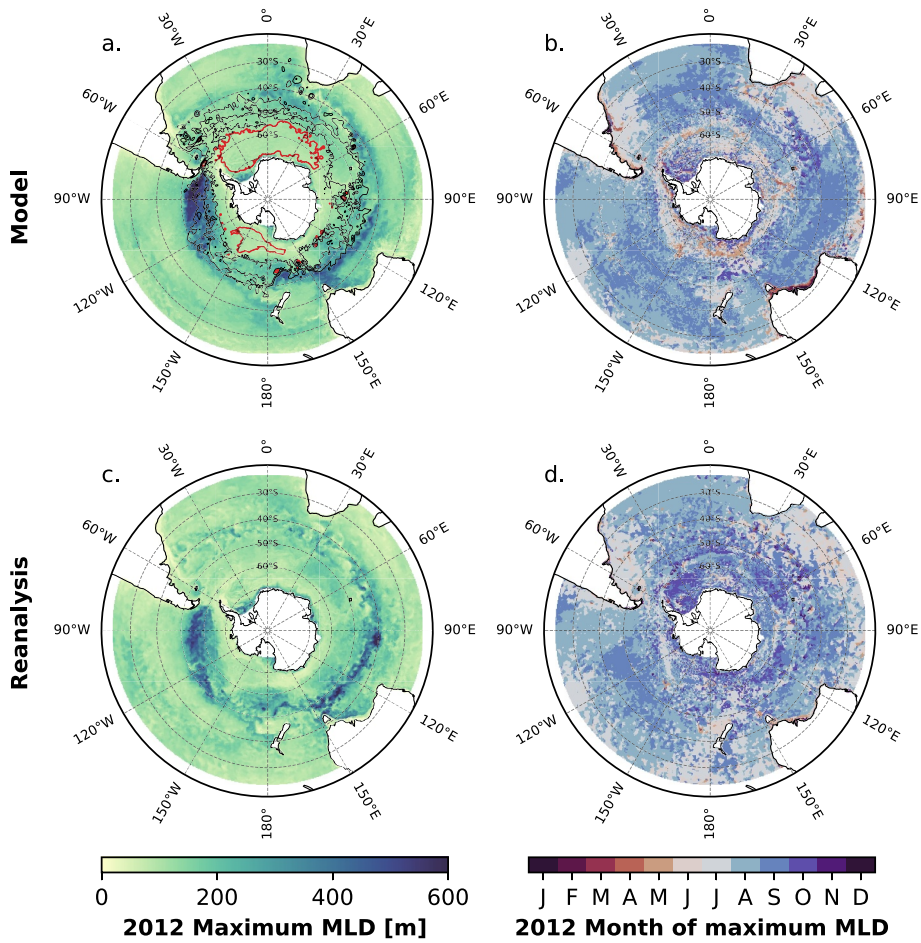

Figure 1. The maximum mixed layer depth (MLD) in 2012 (a) simulated by the forced model and (c) estimated by reanalysis. The timing of the MLD maximum is shown in (b, d). The red countours in (a) are the 20 Sv streamlines of the subpolar gyres. The black contours in (a) are the −10, −60, −110 Sv streamlines of the ACC.

thermocline, where the base of the late-winter mixed layer is adopted as a non-seasonal upper boundary (e.g., J. C. Marshall et al., 1993).

Figures 1a and 1c show the maximum mixed layer depth (MLD) of the Southern Ocean in 2012 from a forced model and reanalysis respectively (details are given in Section 2). A feature of the MLD in the Southern Ocean is its variation along the Antarctic Circumpolar Current (ACC). The maximum MLD varies between 100 and 500 m along the ACC's time-averaged streamlines for 2012 and this could influence ventilation timing in the Southern Ocean. Figure 1a shows the −10, −60, and −110 Sv (1 Sv = 10^6 m^3 s^{-1}) streamlines of the ACC (black) alongside the 20 Sv streamlines of the subpolar gyres. Stommel's demon relies on the net movement of subducted water to regions with a similar or deeper maximum MLD. In the ACC, water that subducts outside of late winter may escape re-entrainment by advecting to an area with a shallower maximum MLD. It is also possible that the substantial mesoscale eddy activity of the Southern Ocean will affect the ventilation process (Kwon, 2013; Kamenkovich et al., 2017; D. Marshall, 1997; Sallée et al., 2010).

We use extensive backwards-in-time trajectories to study the important sites and timing of all ventilation in the Southern Ocean. We also take the unique opportunity to compare the properties of shelf-ventilated and off-shelf-ventilated waters using data from a single experiment.

2. Numerical Simulation and Lagrangian Trajectory Analysis

We use backwards-in-time Lagrangian trajectory analysis in a forced ocean-sea-ice model. Full details of the numerical simulation are given in MacGilchrist et al. (2020) and only essential details are provided here. The

numerical simulation is an implementation of the NEMO model (Madec et al., 2019) coupled with the LIM-2 sea-ice model (Bouillon et al., 2009) and was carried out as part of the Drakkar project (Barnier et al., 2006). The ORCA025 configuration is used, which has a horizontal resolution of 1/4° (~12 km at 65°S and refines with latitude) and 75 irregular vertical model levels. The model is "eddy-permitting," meaning that only the largest mesoscale eddies are resolved. The simulation runs from 1958 to 2015 and is forced with Drakkar Forcing Set 5.2 (Dussin et al., 2016).

Figure 1 compares the forced model to reanalysis from ORAS5 (Zuo et al., 2019) for 2012. The forced model is able to reproduce a similar maximum MLD at a similar time of the year to the observationally constrained reanalysis. Throughout this study, we define the MLD as the depth where the potential density (reference pressure of 0 dbar) is within 0.01 of the 10 m depth value. The MLD is deep to the west of the Drake Passage and south of Australia and the deepest mixed layers occur between August and September. This is in agreement with previous studies (Buongiorno Nardelli et al., 2017; de Boyer Montégut et al., 2004; Dong et al., 2008; Hanawa & Talley, 2001; Sallée et al., 2008, 2010). One notable discrepancy is the thin regions of summer maxima (approximately April) that are visible in the forced model. This is not a consistent feature in the years before 2012 and may arise from anomalous wind forcing in the simulation that year.

The trajectories are calculated using the Lagrangian trajectory code, TRACMASS v7.1 (Aldama-Campino et al., 2020). TRACMASS analytically calculates the trajectory through each model grid cell by assuming that each component of the three dimensional velocity field varies linearly with its respective direction (Blanke & Raynaud, 1997). The trajectories are purely advective and calculated using model velocities that are interpolated between successive 5-day-mean velocity fields. By assuming that the velocity field remains stationary between the intermediate time steps, TRACMASS can calculate approximately mass-conserving trajectories (Döös et al., 2017). NEMO is an incompressible model, so the volume associated with each trajectory is approximately conserved.

We evaluate backwards-in-time trajectories for all interior water that is south of 25°S on the 16 December 2012. Each trajectory has an associated subvolume with a maximum volume of 10^9 m^3. Over 480 million trajectories are calculated, meaning there are significantly more trajectories than there are grid cells. Backwards-in-time trajectories reveal the advective history for each of these subvolumes. The earliest point in a subvolume's history is the most recent occurrence of one of the following:

- It lies in the mixed layer (*Ventilated*);
- It is located north of 25°S;
- It is more than 30 years old.

In this study, we focus on trajectories with histories starting under the first condition ("ventilated" trajectories hereafter). These are the subvolumes that ventilate south of 25°S between 1982 and 2012 and then remain in the ocean interior of this region until the 16th December 2012.

3. Results

In total, 5.80×10^{16} m^3 of water (62 million trajectories) are ventilated in our experiment via advective pathways. Figure 2a shows the age distribution of the ventilated volume. During 2012, the mean MLD is largest in August (Figure 2b) and in our experiment 34% (2.0×10^{16} m^3) of the ventilated volume subducts after this date. These ventilations are "short term" because they may not escape seasonal re-entrainment. The remaining 66% (3.8×10^{16} m^3) of the ventilated volume have escaped re-entrainment. We will be considering the statistics of these "long term" ventilations for the remainder of this article.

In Figure 2a, there is noticeable inter-annual variabilty in ventilation which may originate from variations in subduction, re-entrainment or the interior circulation. This suggests that the Southern Ocean is more receptive to surface conditions in specific years of its history. Decadal variability, which may be significant in the Southern Ocean (e.g., Ting & Holzer, 2017; Waugh et al., 2013; Waugh et al., 2019), cannot be resolved in our 30 year experiment.

Throughout the study, we consider statistics that are aggregated by horizontal position. A single trajectory has two important locations associated with it:

- Their final position: the subvolume's location on the 16th December 2012,

10.1029/2023GL106716

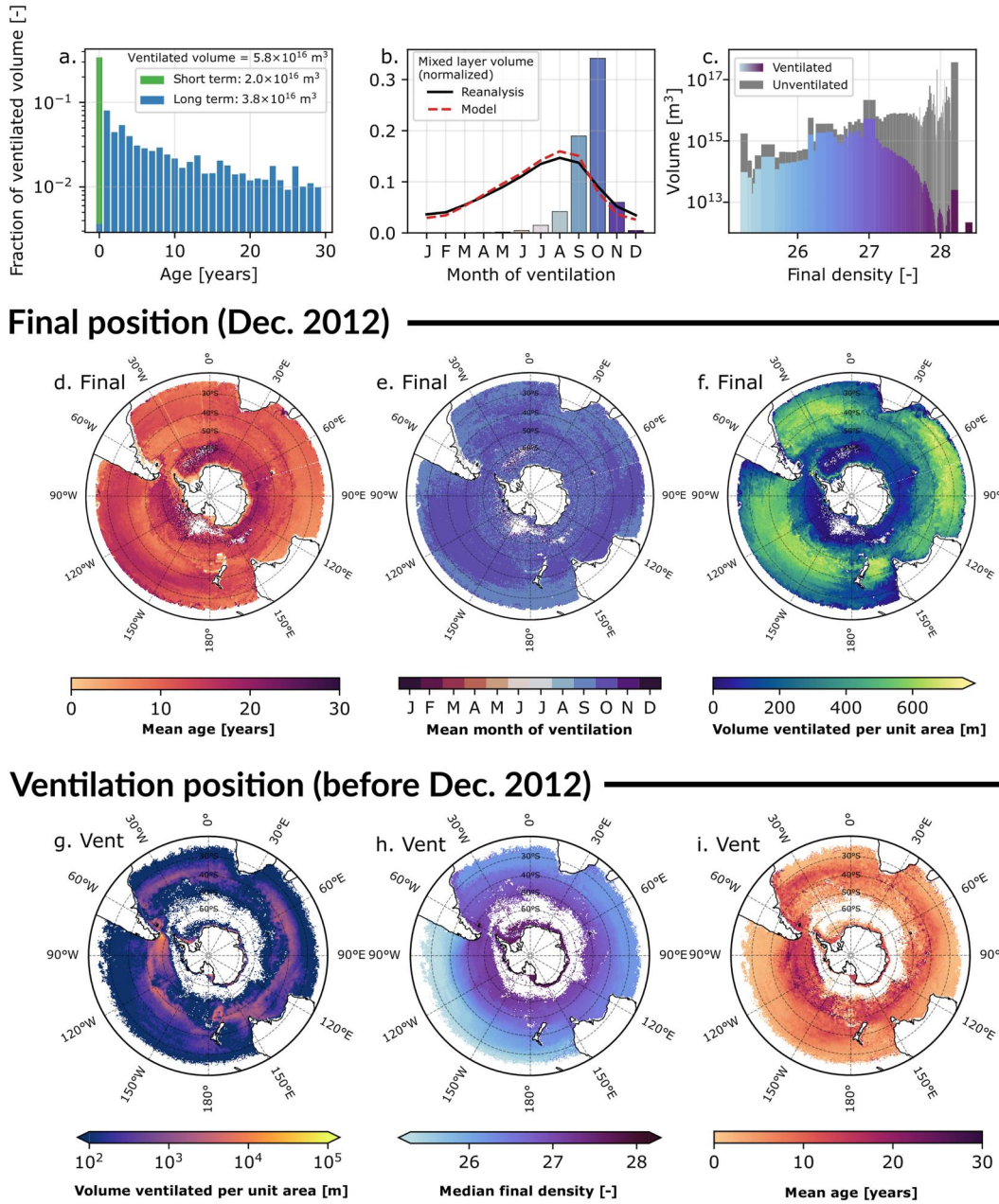

Figure 2. (a) The age distribution of the ventilated trajectories. (b) The ventilated volume aggregated by month and the 2012 mixed layer volume distribution. (c) The ventilated and unventilated volume aggregated by the final density. (d–f) The mean age, mean month of ventilation and ventilated volume aggregated by final position. (g–i) The ventilated volume, median of the final density, and the mean age aggregated by ventilation position.

- Their ventilation position: where the subvolume most recently subducted before the 1st August 2012 (MLD maximum).

We use this terminology throughout the article and label all figures with "Final" and "Vent" accordingly. There are also two important densities, the potential density at subduction (subduction density hereafter) and the approximate neutral density of the subvolume in its final position (final density hereafter). The neutral density is estimated by calculating approximate neutral density surfaces (ω-surfaces) using the methodology of Stanley et al. (2021). Ideally, approximately neutral density surfaces would be used for the subduction density as well, but

calculating consistent surfaces for all time intervals was too computationally expensive. Both the densities use a reference pressure of 0 dbar and agree near the ocean surface.

3.1. Stommel's Demon in the Southern Ocean

We find that the timing of ventilation in the Southern Ocean is highly seasonal. In Figure 2b we aggregate all of the ventilated trajectories by their month of ventilation. The majority of subduction occurs between August and November. Everywhere in the Southern Ocean ventilates at approximately the same time of year (Figure 2e). Just like in the North Atlantic (MacGilchrist et al., 2021), the common months of ventilation are when the mixed layer is shoaling. There are so few cases of subduction before July that all sub-regions considered in this study show a similarly seasonal distribution. This is strong evidence that Stommel's Demon operates in the Southern Ocean.

The mean trajectory age for each final horizontal position is shown in Figure 2d. Water in the subpolar gyres is found to be particularly old (over 20 years) toward the center of the gyres. The white spaces in the center of the gyre inform us that no subvolumes have ventilated. Figure 2f shows that, compared to the Antarctic margins and the ACC, the gyre basins are poorly ventilated regions when considering a 30 year timescale of ventilation. In Section 3.3, we investigate the partial ventilation of the Weddell Gyre.

3.2. Ventilation Sites and Their Properties

We now aggregate the trajectories by their horizontal location of ventilation to identify the common sites of ventilation and the properties of water that ventilates there. Figure 2g shows the volume ventilated at each ventilation position. There is practically no ventilation within the subpolar gyres and ventilation primarily occurs on the continental shelf or at the northern front of the ACC. Any water that subducts within the subpolar gyres is swiftly re-entrained by the dynamic mixed layer. The center of the subpolar gyres may be exclusive hotspots for upwelling into the mixed layer, which could be revealed using an equivalent forwards-in-time experiment trajectory experiment. Alternatively, the centre of the subpolar gyres offer ventilation via diffusive pathways which could be seens in tracer dye experiments similar to Solodoch et al. (2022).

In the open ocean, there is circumpolar ventilation along the northern front of the ACC and the zonal symmetry is broken by several ventilation hotspots (Figure 2g). The ventilation hotspots roughly align with subduction hotspots from observational studies (e.g., Buongiorno Nardelli et al., 2018; Morrison et al., 2022; Sallée et al., 2010, 2012) and align with areas of deep convection (Figure 1a). In Section 3.4, we assess the significance of the ventilation hotspots.

Figure 2h shows the median final density of the subvolumes based on their ventilation position. This indicates the eventual density of the water that ventilates at these sites. The lightest water masses ventilate in the Pacific sector and as expected, the densest waters in the Southern Ocean ventilate on the Antarctic shelf and the least dense waters ventilate north of the ACC. This result is not trivial since climate models can exaggerate the frequency of open-ocean deep-convection events (Heuzé et al., 2015; Reintges et al., 2017). The mean age of a subvolume also varies significantly with the location of ventilation (Figure 2i). Subvolumes that ventilate in areas with deep mixed layers (e.g., west of the Drake Passage) have a mean age between 10 and 20 years. Elsewhere, subvolumes typically have a mean age between 0 and 10 years.

3.3. Ventilation of the Weddell Gyre

We now only consider trajectories that have a final position within the 10 Sv streamline of the Weddell Gyre. The two important sites of ventilation are: the Antarctic Shelf and west of the Drake Passage (Figure 3a) where the maximum MLD is deep (Figure 1a). Studying both the mean age (Figure 3c) and the average final density (Figure 3d) reveals discrete sources for water of specific density or age in the Weddell Gyre. The youngest waters (5 years or younger) ventilate close to the Weddell Gyre in the southern limits of the Weddell Sea. These young waters have a median final density between 27.5 and 27.75. A similarly young population of water also ventilates in the ACC between 150 and 90°W. These waters end up as some of the lowest density water masses in the Weddell Gyre interior (approximately 27.25).

The densest waters (above 27.75) found in the Weddell Gyre ventilate on the Antarctic shelf with a mean age between 10 and 20 years. Similarly dense but much older water (25–30 years) also ventilate at the site of deep convection west of the Drake Passage (90–60°W).

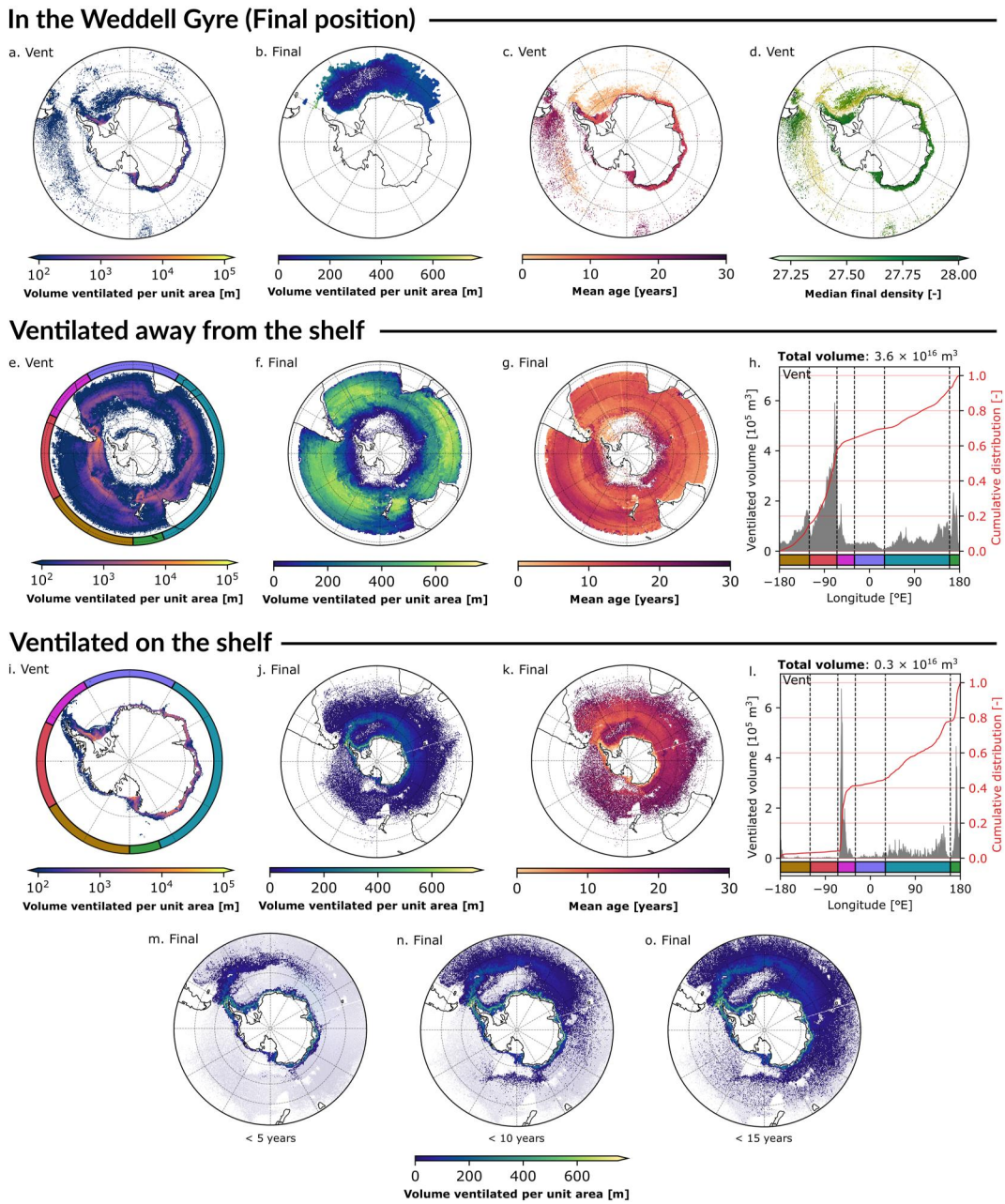

Figure 3. The statistics of ventilated trajectories that have a final position in the Weddell Gyre, ventilated away from the Antarctic shelf, or ventilated on the Antarctic shelf. All quantities are calculated and presented in the same way as Figure 2. The gray bars in (h, l) show the longitudinal variation of off-shelf and on-shelf ventilated volume respectively. The red line is the cumulative distribution function. The colored bars span the same longitudinal range as the colored arcs in (e, i). (m–o) The ventilated volume for trajectories that are less than 5, 10, and 15 years old.

3.4. Ventilation Away From the Shelf

We now only consider trajectories that ventilate away from the Antarctic shelf. A trajectory is assumed to have ventilated away from the shelf if its ventilation position is outside the closed 2,000 m isobath surrounding Antarctica. Figure 3f shows the final distribution of these ventilation subvolumes. Few subvolumes end up in the subpolar gyres or on the shelf. Although there are clear hotspots of ventilation (Figure 3e), the recently subducted water is efficiently spread out across the ACC and north of it, in agreement with Sallée et al. (2010), Sallée

et al. (2012), and Jones et al. (2016). These hotspots have been argued to originate from bathymetric constraints which affects the MLD distribution, steers the circulation, and modifies the isopycnal tilt (Sallée et al., 2010).

Figure 3h shows how the ventilated volume varies with the longitude of ventilation. Two subduction hotspots dominate the ventilation between 180 and 65°W, where 60% of ventilation occurs. Around the remainder of Antarctica, the hotspots are less apparent as ventilation varies smoothly with longitude, suggesting a more circumpolar pattern of ventilation. This result suggests that subduction hotspots offer a partial view of open Southern Ocean ventilation.

3.5. Ventilation on the Shelf

We now only consider trajectories that ventilate on the Antarctic shelf, within the closed 2,000 m isobath surrounding Antarctica (Figure 3i). On a 30 year timescale, shelf-ventilated waters are mostly contained south of the ACC but can travel to more northerly latitudes (Figure 3j). In Figure 3k, the youngest subvolumes in the interior ocean are found on the western boundary of the Weddell Gyre (60°W). This region is the most significant export pathway for shelf-ventilated water. Another weaker pathway follows the western boundary current of the Ross Gyre. Within five years of ventilating on the shelf (Figure 3m), some subvolumes have wrapped around the northern limb of the Weddell Gyre and started to traverse the western boundary of the Ross Gyre (160°E). Within 10 years (Figure 3n), trajectories have started to wrap around the Ross Gyre and be dispersed by the ACC. Similar export pathways have been found in the passive tracer experiments of Solodoch et al. (2022).

The on-shelf ventilation is more localized than the off-shelf ventilation (Figure 3l). Approximately 40% of the shelf's ventilation takes place on the eastern side of the Antarctic Peninsula (65–30°W) and an additional 20% takes place in the west Ross Sea (160–180°E). These ventilation hotpots align with two of four observed sites of AABW formation on the Antarctic shelf (Purkey et al., 2018). The other two sites (Prydz Bay and the Adélie Coast) are not clearly pronounced. This may be because insufficient dense water is being formed at these sites in the model or alternatively, the dense water that forms at these sites is swiftly re-entrained elsewhere along the Antarctic coastline. The remaining 40% of ventilation is evenly spread over East Antarctica (30–160°E). Little ventilation takes place in West Antarctica (180–65°W), which aligns with the "warm shelf" described in Thompson et al. (2018).

3.6. Separability of Shelf-Ventilated Water

Almost all of the statistics considered so far have been aggregated by horizontal position and we have ignored vertical variations. This raises the question, how much overlap is there of shelf-ventilated and off-shelf-ventilated water when considering ventilation on a 30 year timescale?

Figure 4a shows what fraction of the recorded ventilation in a water column originates from the Antarctic shelf. Most fluid columns in the Southern Ocean can be approximated as entirely ventilated on the shelf (100%, blue) or entirely ventilated off the shelf (0%, red). The interface between these two classes is narrow and aligns closely with the southern front of the ACC (illustrated by the −10 Sv streamline in Figure 4a). In Section 3.5, we found that shelf-ventilated trajectories can travel north of the ACC in 30 years, but Figure 4 suggests that the volume of these trajectories is negligible compared to the volume of off-shelf-ventilated water.

This result highlights the different rates of ventilation for shelf-ventilated and off-shelf-ventilated water. In 30 years, approximately 10 times more water ventilates in the open ocean (3.6×10^{16} m^3) compared to the Antarctic shelf (0.3×10^{16} m^3), even though shelf-ventilated abyssal waters make up most of the Southern Ocean (Figure 2c). A small fraction of the dense water ventilates and is approximately contained south of the ACC.

3.7. Density Distribution

Finally, we consider the structure of Southern Ocean ventilation in density-latitude space (Figures 4c–4j). The circumpolar statistics are considered alongside the statistics of the Atlantic, Indian, and Pacific sectors (Figure 4). Following on from the previous subsection, a line in density-latitude space separates shelf-ventilated and off-shelf-ventilated water. The line is not well defined at latitudes greater than 45°S, because so little shelf-ventilated water reaches this latitude on a 30 year timescale.

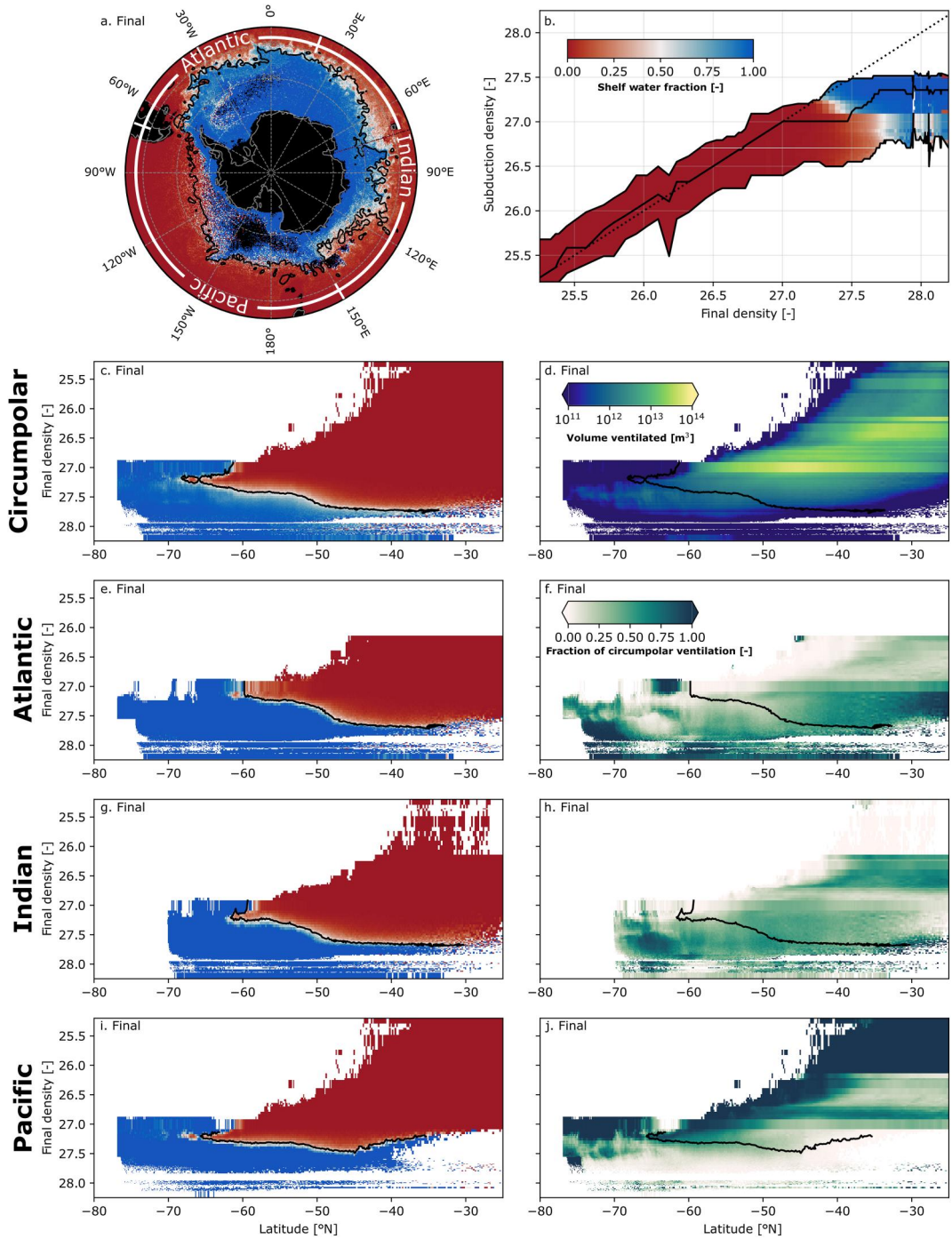

Figure 4. (a) The shelf water fraction aggregated by final position. The black contour is the −10 Sv streamline of the ACC in December 2012. (b) Comparing the subduction density to the final density. The central line shows the median subduction density. The upper and lower lines show the respective 5th and 95th percentile. (c, e, g, i) The shelf water fraction in density-latitude space across various sectors of the Southern Ocean. (d, f, h, j) Ventilation in density-latitude space across the same sectors. The black line in (c–j) is the approximate boundary between shelf-ventilated and off-shelf-ventilated waters.

Most shelf-ventilated water has a final density between 27.25 and 28.00; off-shelf-ventilated water has a final density between 25.50 and 27.75 (Figure 4d). The densest shelf-ventilated waters are found in the Atlantic sector (Figure 4f), while the lightest shelf-ventilated waters are in the Pacific (Figure 4j). Similarly, the lowest density off-shelf-ventilated waters are found in the Pacific and the highest density subvolumes are found in the Atlantic. This suggests that the lower density Pacific-ventilated waters (Figure 2h) remain in the Pacific.

To understand the trajectory of these volumes in density space, we need to see their density transformation in the ocean interior. Figure 4b compares the subduction density to the final density. The central line shows the median subduction density while the lower and upper lines show the 5th and 95th percentile. These lines represent the envelope of transformation that 90% of the subvolumes experience and the color shows the shelf water fraction.

A fraction of any transformation found in this study may be numerical and could originate from the following: cumulative errors in the trajectory calculation (van Sebille et al., 2018), the approximation of neutral density surfaces (Stanley et al., 2021), and implicit model mixing (Griffies et al., 2000; Lee et al., 2002). Megann (2018) found implicit mixing to be similar to or greater in magnitude than parameterized mixing in a related NEMO ocean model.

Water with a final density less than 27.0 has a similar median subduction density (Figure 4b). On average, little transformation takes place and the spread of the subduction density indicates that the range of transformation is within 0.5 of the median. In contrast, almost all water with a final density greater than 27.0 has become more dense since subduction. The most extreme cases of densification originate from shelf-ventilated trajectories with a final density greater than 27.75 and an age greater than 5 years. In Section 3.3, some of this transformed water is identified in the Weddell Gyre (Figure 3d). Poorly ventilated dense water and interior densification of lighter water masses indicate that reserves of denser bottom water are being eroded by interior transformation processes. Presumably, the shelf-ventilated waters interact with dense bottom water as they enter the subpolar gyres and/or follow the ACC (Figure 3n). Studies indicate this may be happening in the Southern Ocean as a consequence of climate change (e.g., Li et al., 2023; Purkey & Johnson, 2010; Zhou et al., 2023) via glacial melt. The forced model run does include climate change and glacial melt but the effect could be exaggerated by model biases or drifts similar to those found in climate models (Heuzé, 2021; Purich & England, 2021).

4. Conclusions

We have used backwards-in-time trajectories to study a 30 year history of the Southern Ocean and identified spatial and temporal patterns of ventilation that will simplify conceptual models. We found conclusive evidence that ventilation in the Southern Ocean is highly seasonal. Despite significant variations of the MLD along the streamlines of the ACC and significant eddy activity, Stommel's demon only allows ventilation between August and November. There is also evidence of inter-annual variability (Figure 2a); future studies should investigate if an inter-annual demon operates as well using the methodology of MacGilchrist et al. (2021).

We identified spatial patterns of ventilation in the open Southern Ocean. Circumpolar ventilation takes place along the northern front of the ACC and the zonal symmetry is broken by several ventilation hotspots (Figure 2g). The hotspots of ventilation overlap with sites of deep convection (Figure 1a) and local regions of subduction from observational studies (Buongiorno Nardelli et al., 2017; Sallée et al., 2010, 2012) but they only account for 60% of open-ocean ventilation. Circumpolar patterns of ventilation and ventilation hotspots have similar levels of influence on the Southern Ocean.

Almost no ventilation takes place in the subpolar gyres (Figure 2g). Any subduction that occurs within the streamlines of the gyres is swiftly re-entrained by the following mixed layer seasonal cycle. It is worth remembering that the experiment only reveals advective pathways of ventilation, so it is possible that ventilation does take place in the gyre centre but via a diffusive mechanism. This could be tested using dedicated dye experiments similar to Solodoch et al. (2022). On a 30 year timescale, water in the Weddell Gyre ventilates remotely. The subvolumes primarily ventilate on the Antarctic shelf but also ventilate west of the Drake Passage where the mixed layer is deep (Figure 3a).

The Antarctic shelf is where the densest water masses of the Southern Ocean ventilate and we find that 40% of shelf ventilation occurs on the Antarctic Peninsula and 20% in the west Ross sea (Figure 3l). These are two known sites of AABW formation on the Antarctic shelf but other sites are not clear in the model. The remaining 40% of ventilation is spread over East Antarctica. Shelf-ventilated waters are exported to the Southern Ocean via two export pathways, parallel to the western boundaries of the Weddell and Ross Gyre (Figures 3m and 3n) in agreement with passive tracer experiments (with diffusion) by Solodoch et al. (2022).

Abyssal waters north of the ACC hardly ventilate on a 30 year timescale (Figure 2c) because shelf-ventilated waters need significantly more time to cross the ACC. In contrast, off-shelf-ventilated waters experience more rapid ventilation in the open Southern Ocean but rarely travel south of the ACC (Figure 2f). Consequently, the

southern boundary of the ACC approximately separates columns of shelf-ventilated and off-shelf-ventilated water (Figure 4a). This approximation predicts the area of effect for climate change in the Southern Ocean on anthropogenic timescales. Off-shelf-ventilated waters change quickly over a large area, while denser shelf-ventilated waters modify slowly but accumulate in the smaller area south of the ACC.

Finally, we compared the subduction density to the final density. On average, water with a final density lower than 27.0 experiences little transformation. Almost all water with a final density greater than 27.5 experiences densification after subduction (Figure 4b). On a thirty year timescale, the densest water masses do not form within the mixed layer; Instead, the dense water masses are being consumed to densify lighter water masses which have made contact with the mixed layer. This result is consistent with a warming world that is forming less AABW (e.g., Li et al., 2023; Purkey & Johnson, 2010; Zhou et al., 2023) because of glacial melt but could be exaggerated by inaccuracies from the eddy-permitting model or the trajectory calculation. Running similar experiments on higher resolution models and reanalysis products may help to determine how realistic this climate change signal is.

Data Availability Statement

Data for the trajectories used in this study are archived on Zenodo (Styles et al., 2023b) alongside the calculated statistics. The software used to analyze the model outputs is also archived on Zenodo (Styles et al., 2023a).

Acknowledgments
The work was financially supported by the Natural Environment Research Council NE/S007474/1. Partial support was provided by the European Union's Horizon 2020 research and innovation programme under grant agreement No. 821001. Mike Bell was supported by the Met Office Hadley Centre Climate Programme funded by BEIS and Defra and funding for the Met Office's public weather service. This work used JASMIN, the UK collaborative data analysis facility. We would also like to thank Andrew Wells and Alberto Naveira Garabato for their helpful discussions.

References

Aldama-Campino, A., Döös, K., Kjellsson, J., & Jönsson, B. (2020). *TRACMASS: Formal release of version 7.0*. Zenodo. https://doi.org/10.5281/zenodo.4337926

Barnier, B., Madec, G., Penduff, T., Molines, J. M., Treguier, A. M., Le Sommer, J., et al. (2006). Impact of partial steps and momentum advection schemes in a global ocean circulation model at eddy-permitting resolution. *Ocean Dynamics*, *56*(5–6), 543–567. https://doi.org/10.1007/s10236-006-0082-1

Blanke, B., & Raynaud, S. (1997). Kinematics of the Pacific equatorial undercurrent: An eulerian and Lagrangian approach from GCM results. *Journal of Physical Oceanography*, *27*(6), 1038–1053. https://doi.org/10.1175/1520-0485(1997)027⟨1038:KOTPEU⟩2.0.CO;2

Bopp, L., Le Quéré, C., Heimann, M., Manning, A. C., & Monfray, P. (2002). Climate-induced oceanic oxygen fluxes: Implications for the contemporary carbon budget. *Global Biogeochemical Cycles*, *16*(2), 6-1–6-13. https://doi.org/10.1029/2001GB001445

Bouillon, S., Morales Maqueda, M. Á., Legat, V., & Fichefet, T. (2009). An elastic–viscous–plastic sea ice model formulated on Arakawa B and C grids. *Ocean Modelling*, *27*(3), 174–184. https://doi.org/10.1016/j.ocemod.2009.01.004

Buongiorno Nardelli, B., Guinehut, S., Verbrugge, N., Cotroneo, Y., Zambianchi, E., & Iudicone, D. (2017). Southern ocean mixed-layer seasonal and interannual variations from combined satellite and in situ data. *Journal of Geophysical Research: Oceans*, *122*(12), 10042–10060. https://doi.org/10.1002/2017JC013314

Buongiorno Nardelli, B., Mulet, S., & Iudicone, D. (2018). Three-dimensional ageostrophic motion and water mass subduction in the southern ocean. *Journal of Geophysical Research: Oceans*, *123*(2), 1533–1562. https://doi.org/10.1002/2017JC013316

de Boyer Montégut, C., Madec, G., Fischer, A. S., Lazar, A., & Iudicone, D. (2004). Mixed layer depth over the global ocean: An examination of profile data and a profile-based climatology. *Journal of Geophysical Research*, *109*(C12), C12003. https://doi.org/10.1029/2004JC002378

Dong, S., Sprintall, J., Gille, S. T., & Talley, L. (2008). Southern Ocean mixed-layer depth from Argo float profiles. *Journal of Geophysical Research*, *113*(C6), C06013. https://doi.org/10.1029/2006JC004051

Döös, K., Jönsson, B., & Kjellsson, J. (2017). Evaluation of oceanic and atmospheric trajectory schemes in the TRACMASS trajectory model v6.0. *Geoscientific Model Development*, *10*(4), 1733–1749. https://doi.org/10.5194/gmd-10-1733-2017

Dussin, R., Barnier, B., Brodeau, L., & Molines, J. M. (2016). *Drakkar forcing set DFS5* (Tech. Rep.). Laboratoire de glaciologie et géophysique de l'environnement. Retrieved from https://www.drakkar-ocean.eu/publications/reports/report_DFS5v3_April2016.pdf

Frölicher, T. L., Sarmiento, J. L., Paynter, D. J., Dunne, J. P., Krasting, J. P., & Winton, M. (2015). Dominance of the Southern Ocean in anthropogenic carbon and heat uptake in CMIP5 models. *Journal of Climate*, *28*(2), 862–886. https://doi.org/10.1175/JCLI-D-14-00117.1

Gebbie, G., & Huybers, P. (2010). Total matrix intercomparison: A method for determining the geometry of water-mass pathways. *Journal of Physical Oceanography*, *40*(8), 1710–1728. https://doi.org/10.1175/2010JPO4272.1

Griffies, S. M., Pacanowski, R. C., & Hallberg, R. W. (2000). Spurious diapycnal mixing associated with advection in a z-coordinate ocean model. *Monthly Weather Review*, *128*(3), 538–564. https://doi.org/10.1175/1520-0493(2000)128⟨0538:SDMAWA⟩2.0.CO;2

Hanawa, K., & Talley, L. D. (2001). Chapter 5.4 mode waters. In G. Siedler, J. Church, & J. Gould (Eds.), *International geophysics* (Vol. 77, pp. 373–386). Academic Press. https://doi.org/10.1016/S0074-6142(01)80129-7

Heuzé, C. (2021). Antarctic bottom water and North Atlantic deep water in CMIP6 models. *Ocean Science*, *17*(1), 59–90. https://doi.org/10.5194/os-17-59-2021

Heuzé, C., Ridley, J. K., Calvert, D., Stevens, D. P., & Heywood, K. J. (2015). Increasing vertical mixing to reduce Southern Ocean deep convection in NEMO3.4. *Geoscientific Model Development*, *8*(10), 3119–3130. https://doi.org/10.5194/gmd-8-3119-2015

Jones, D. C., Boland, E., Meijers, A. J., Forget, G., Josey, S. A., Sallee, J.-B., & Shuckburgh, E. (2019). Heat distribution in the southeast Pacific is only weakly sensitive to high-latitude heat flux and wind stress. *Journal of Geophysical Research: Oceans*, *124*(12), 8647–8666. https://doi.org/10.1029/2019JC015460

Jones, D. C., Meijers, A. J. S., Shuckburgh, E., Sallée, J.-B., Haynes, P., McAufield, E. K., & Mazloff, M. R. (2016). How does subantarctic mode water ventilate the Southern Hemisphere subtropics? *Journal of Geophysical Research: Oceans*, *121*(9), 6558–6582. https://doi.org/10.1002/2016JC011680

Kamenkovich, I., Garraffo, Z., Pennel, R., & Fine, R. A. (2017). Importance of mesoscale eddies and mean circulation in ventilation of the Southern Ocean. *Journal of Geophysical Research: Oceans*, *122*(4), 2724–2741. https://doi.org/10.1002/2016JC012292

Kwon, E. Y. (2013). Temporal variability of transformation, formation, and subduction rates of upper Southern Ocean waters. *Journal of Geophysical Research: Oceans*, *118*(11), 6285–6302. https://doi.org/10.1002/2013JC008823

Lee, M.-M., Coward, A. C., & Nurser, A. J. G. (2002). Spurious diapycnal mixing of the deep waters in an eddy-permitting global ocean model. *Journal of Physical Oceanography*, *32*(5), 1522–1535. https://doi.org/10.1175/1520-0485(2002)032⟨1522:SDMOTD⟩2.0.CO;2

Li, Q., England, M. H., Hogg, A. M., Rintoul, S. R., & Morrison, A. K. (2023). Abyssal ocean overturning slowdown and warming driven by Antarctic meltwater. *Nature*, *615*(7954), 841–847. https://doi.org/10.1038/s41586-023-05762-w

Liu, L. L., & Huang, R. X. (2012). The global subduction/obduction rates: Their interannual and decadal variability. *Journal of Climate*, *25*(4), 1096–1115. https://doi.org/10.1175/2011JCLI4228.1

MacGilchrist, G. A., Johnson, H. L., Lique, C., & Marshall, D. P. (2021). Demons in the North Atlantic: Variability of deep ocean ventilation. *Geophysical Research Letters*, *48*(9), 1–9. https://doi.org/10.1029/2020GL092340

MacGilchrist, G. A., Johnson, H. L., Marshall, D. P., Lique, C., Thomas, M., Jackson, L. C., & Wood, R. A. (2020). Locations and mechanisms of ocean ventilation in the high-latitude North Atlantic in an eddy-permitting ocean model. *Journal of Climate*, *33*(23), 10113–10131. https://doi.org/10.1175/JCLI-D-20-0191.1

Madec, G., Bourdallé-Badie, R., Chanut, J., Samson, E. C., Coward, A., Ethé, C., et al. (2019). NEMO ocean engine. *Zenodo*. https://doi.org/10.5281/zenodo.1464816

Marshall, D. (1997). Subduction of water masses in an eddying ocean. *Journal of Marine Research*, *55*(2), 201–222. https://doi.org/10.1357/0022240973224373

Marshall, J. C., Williams, R. G., & Nurser, A. J. G. (1993). Inferring the subduction rate and period over the North Atlantic. *Journal of Physical Oceanography*, *23*(7), 1315–1329. https://doi.org/10.1175/1520-0485(1993)023⟨1315:ITSRAP⟩2.0.CO;2

Megann, A. (2018). Estimating the numerical diapycnal mixing in an eddy-permitting ocean model. *Ocean Modelling*, *121*, 19–33. https://doi.org/10.1016/j.ocemod.2017.11.001

Morrison, A. K., Waugh, D. W., Hogg, A. M., Jones, D. C., & Abernathey, R. P. (2022). Ventilation of the Southern Ocean pycnocline. *Annual Review of Marine Science*, *14*(1), 405–430. https://doi.org/10.1146/annurev-marine-010419-011012

Purich, A., & England, M. H. (2021). Historical and future projected warming of Antarctic shelf bottom water in CMIP6 models. *Geophysical Research Letters*, *48*(10), e2021GL092752. https://doi.org/10.1029/2021GL092752

Purkey, S. G., & Johnson, G. C. (2010). Warming of global abyssal and deep southern ocean waters between the 1990s and 2000s: Contributions to global heat and sea level rise budgets. *Journal of Climate*, *23*(23), 6336–6351. https://doi.org/10.1175/2010JCLI3682.1

Purkey, S. G., Smethie, W. M., Gebbie, G., Gordon, A. L., Sonnerup, R. E., Warner, M. J., & Bullister, J. L. (2018). A synoptic view of the ventilation and circulation of Antarctic bottom water from chlorofluorocarbons and natural tracers. *Annual Review of Marine Science*, *10*(1), 503–527. https://doi.org/10.1146/annurev-marine-121916-063414

Reintges, A., Martin, T., Latif, M., & Park, W. (2017). Physical controls of Southern Ocean deep-convection variability in CMIP5 models and the Kiel climate model. *Geophysical Research Letters*, *44*(13), 6951–6958. https://doi.org/10.1002/2017GL074087

Sallée, J.-B., Matear, R. J., Rintoul, S. R., & Lenton, A. (2012). Localized subduction of anthropogenic carbon dioxide in the Southern Hemisphere oceans. *Nature Geoscience*, *5*(8), 579–584. https://doi.org/10.1038/ngeo1523

Sallée, J.-B., Morrow, R., & Speer, K. (2008). Eddy heat diffusion and subantarctic mode water formation. *Geophysical Research Letters*, *35*(5), L05607. https://doi.org/10.1029/2007GL032827

Sallée, J.-B., Speer, K., Rintoul, S., & Wijffels, S. (2010). Southern Ocean thermocline ventilation. *Journal of Physical Oceanography*, *40*(3), 509–529. https://doi.org/10.1175/2009JPO4291.1

Sarmiento, J. L., Gruber, N., Brzezinski, M. A., & Dunne, J. P. (2004). High-latitude controls of thermocline nutrients and low latitude biological productivity. *Nature*, *427*(6969), 56–60. https://doi.org/10.1038/nature02127

Solodoch, A., Stewart, A. L., Hogg, A. M., Morrison, A. K., Kiss, A. E., Thompson, A. F., et al. (2022). How does Antarctic bottom water cross the southern ocean? *Geophysical Research Letters*, *49*(7), e2021GL097211. https://doi.org/10.1029/2021GL097211

Stanley, G. J., McDougall, T. J., & Barker, P. M. (2021). Algorithmic improvements to finding approximately neutral surfaces. *Journal of Advances in Modeling Earth Systems*, *13*(5), e2020MS002436. https://doi.org/10.1029/2020MS002436

Stommel, H. (1979). Determination of water mass properties of water pumped down from the Ekman layer to the geostrophic flow below. *Proceedings of the National Academy of Sciences*, *76*(7), 3051–3055. https://doi.org/10.1073/pnas.76.7.3051

Styles, A. F., MacGilchrist, G., Bell, M. J., & Marshall, D. P. (2023a). Analysis software for "spatial and temporal patterns of southern ocean ventilation". *Zenodo*. https://doi.org/10.5281/zenodo.8413773

Styles, A. F., MacGilchrist, G., Bell, M. J., & Marshall, D. P. (2023b). Data for "spatial and temporal patterns of southern ocean ventilation". *Zenodo*. https://doi.org/10.5281/zenodo.8413705

Talley, L. (2013). Closure of the global overturning circulation through the Indian, Pacific, and southern oceans: Schematics and transports. *Oceanography*, *26*(1), 80–97. https://doi.org/10.5670/oceanog.2013.07

Thompson, A. F., Stewart, A. L., Spence, P., & Heywood, K. J. (2018). The Antarctic slope current in a changing climate. *Reviews of Geophysics*, *56*(4), 741–770. https://doi.org/10.1029/2018RG000624

Ting, Y.-H., & Holzer, M. (2017). Decadal changes in Southern Ocean ventilation inferred from deconvolutions of repeat hydrographies. *Geophysical Research Letters*, *44*(11), 5655–5664. https://doi.org/10.1002/2017GL073788

van Sebille, E., Griffies, S. M., Abernathey, R., Adams, T. P., Berloff, P., Biastoch, A., et al. (2018). Lagrangian ocean analysis: Fundamentals and practices. *Ocean Modelling*, *121*, 49–75. https://doi.org/10.1016/j.ocemod.2017.11.008

Waugh, D. W., Hogg, A. M., Spence, P., England, M. H., & Haine, T. W. N. (2019). Response of Southern Ocean Ventilation to changes in midlatitude westerly winds. *Journal of Climate*, *32*(17), 5345–5361. https://doi.org/10.1175/JCLI-D-19-0039.1

Waugh, D. W., Primeau, F., DeVries, T., & Holzer, M. (2013). Recent changes in the ventilation of the southern oceans. *Science*, *339*(6119), 568–570. https://doi.org/10.1126/science.1225411

Williams, R. G., Marshall, J. C., & Spall, M. A. (1995). Does Stommel's mixed layer "demon" work? *Journal of Physical Oceanography*, *25*(12), 3089–3102. https://doi.org/10.1175/1520-0485(1995)025⟨3089:DSMLW⟩2.0.CO;2

Zhou, S., Meijers, A. J. S., Meredith, M. P., Abrahamsen, E. P., Holland, P. R., Silvano, A., et al. (2023). Slowdown of Antarctic bottom water export driven by climatic wind and sea-ice changes. *Nature Climate Change*, *13*(7), 701–709. https://doi.org/10.1038/s41558-023-01695-4

Zuo, H., Balmaseda, M. A., Tietsche, S., Mogensen, K., & Mayer, M. (2019). The ECMWF operational ensemble reanalysis–analysis system for ocean and sea ice: A description of the system and assessment. *Ocean Science*, *15*(3), 779–808. https://doi.org/10.5194/os-15-779-2019